


# Reversing T Cell Exhaustion by Converting Membrane PD-1 to Its Soluble form in Jurkat Cells; Applying The CRISPR/Cas9 Exon Skipping Strategy

Zeinab Yousefi-Najafabadi, Ph.D.<sup>1,2</sup>, Zohreh Mehmandoostli, Ph.D.<sup>2</sup>, Yazdan Asgari, Ph.D.<sup>1</sup>,  
Saeed Kaboli, Ph.D.<sup>3</sup>, Reza Falak, Ph.D.<sup>4</sup>, Gholam Ali Kardar, Ph.D.<sup>1,2\*</sup> 

1. Department of Medical Biotechnology, School of Advanced Technologies in Medicine, Tehran University of Medical Sciences, Tehran, Iran
2. Immunology, Asthma and Allergy Research Institute (IAARI), Tehran University of Medical Sciences, Tehran, Iran
3. Department of Medical Biotechnology, School of Medicine, Zanjan University of Medical Sciences, Zanjan, Iran
4. Department of Immunology, School of Medicine, Iran University of Medical Sciences, Tehran, Iran

## Abstract

**Objective:** T-cells express two functional forms of the programmed cell death protein 1 (PD-1): membrane (mPD-1) and soluble (sPD-1). The binding of mPD-1 and its ligand (PD-L1) on tumor cells could lead activated lymphocytes toward exhaustion. Selective deletion of the transmembrane domain via alternative splicing of exon-3 in PD-1 mRNA could generate sPD-1. Overexpression of sPD-1 could disrupt the mPD-1/PD-L1 interaction in tumor-specific T cells. We investigated the effect of secreted sPD-1 from pooled engineered and non-engineered T cell supernatant on survival and proliferation of lymphocytes in the tumor microenvironment (TME).

**Materials and Methods:** In this experimental study, we designed two sgRNA sequences upstream and downstream of exon-3 in the *PDCD1* gene. The lentiCRISPRv2 puro vector was used to clone the dual sgRNAs and produce lentiviral particles to transduce Jurkat T cells. Analysis assays were used to clarify the change in PD-1 expression pattern in the pooled (engineered and non-engineered) Jurkat cells. Co-culture conditions were established with PD-L1+ cancer cells and lymphocytes.

**Results:** CRISPR/Cas9 could delete exon-3 of the *PDCD1* gene in the engineered cells based on the tracking of indels by decomposition (TIDE) and interference of CRISPR edit (ICE) sequencing analysis reports. Our results showed a 12% reduction in mPD-1 positive cell population after CRISPR manipulation and increment in sPD-1 concentration in the supernatant. The increased sPD-1 confirmed its positive effect on proliferation of lymphocytes co-cultured with PD-L1+ cancer cells. The survival percent of lymphocytes co-cultured with the pooled cells supernatant was 12.5% more than the control.

**Conclusion:** The CRISPR/Cas9 exon skipping approach could be used in adoptive cell immunotherapies to change PD-1 expression patterns and overcome exhaustion.

**Keywords:** CRISPR-Cas Systems, Exhaustion, Exons, PD-1-PD-L1 Blockade, Programmed Cell Death 1 Receptor

**Citation:** Yousefi-Najafabadi Z, Mehmandoostli Z, Asgari Y, Kaboli S, Falak R, Kardar GA. Reversing T cell exhaustion by converting membrane PD-1 to its soluble form in jurkat cells; applying the CRISPR/Cas9 exon skipping strategy. *Cell J.* 2023; 25(9): 633-644. doi: 10.22074/CELLJ.2023.1999548.1269  
This open-access article has been published under the terms of the Creative Commons Attribution Non-Commercial 3.0 (CC BY-NC 3.0).

## Introduction

The physiological condition of the tumor microenvironment (TME) could lead the tumor-specific T lymphocytes, CD8<sup>+</sup> and CD4<sup>+</sup>, towards exhaustion. The most significant T lymphocyte exhaustion hallmarks, depending on their progenitor or terminal status, are the expression of one or more inhibitory markers such as programmed cell death protein 1 (PD-1), cytotoxic T-lymphocyte-associated protein 4 (CTLA4); T-cell immunoglobulin and mucin-domain containing-3 (TIM3); lymphocyte-activation gene 3 (LAG3); B- and T-lymphocyte attenuator (BTLA); T cell immunoreceptor

with Ig and immunoreceptor tyrosine-based inhibitory motif (ITIM) domains (TIGIT); 2B4; and SLAM family member 6 (SLAMF6) (1-3). Exhaustion could be a transient state in T lymphocytes, and blocking the inhibitory markers or their ligands could distort the inhibitory signalling pathways and reverse this condition (4, 5). The PD-1 protein is the first inhibitory coreceptor expressed on the surface of effector T cells in the TME (6). Therefore, immunotherapy methods that include anti-PD-1/anti-PD-L1 monoclonal antibodies (7), siRNA-mediated down-regulation of PD-1 expression (8), and programmed cell death 1 (*PDCD1*) gene knock-out

Received: 05/April/2023, Revised: 28/May/2023, Accepted: 17/June/2023

\*Corresponding Address: P.O.Box: 14177-55469, Department of Medical Biotechnology, School of Advanced Technologies in Medicine, Tehran University of Medical Sciences, Tehran, Iran  
Email: [gakardar@tums.ac.ir](mailto:gakardar@tums.ac.ir)



Royan Institute  
Cell Journal (Yakhteh)

methods by zinc finger nucleases (ZFNs) (9); clustered regularly interspaced short palindromic repeats and CRISPR-associated protein 9 (CRISPR/Cas9) (10-12) are developed to disrupt the PD-1/PD-L1 axis. These methods could be used with traditional cancer treatments and adoptive cell transfer (ACT) therapies to improve their functions as combinational therapies (13).

Recent studies demonstrated that in addition to the full-length membrane PD-1 isoform (mPD-1), the PD-1 mRNA transcript has four alternative splice variants. In mPD-1, exon-2 is responsible for the extracellular IgV-like domain expression, which is crucial for PD-1/PD-L1 binding. Exon-3 is in charge of transmembrane domain expression. The full-length PD-1 also retains an intracellular domain with an ITIM and an immunoreceptor tyrosine-based switch motif (ITSM) as signalling motifs, by exons 4 and 5. Transformation of PD-1 from the mPD-1 form to the soluble form (sPD-1) is the result of exon-3 deletion due to alternative splicing of the PD-1 mRNA transcript (14). The sPD-1 transcript has prognostic, diagnostic, and therapeutic values and is regarded as a biomarker in human cancers (15). Notably, sPD-1 can block the mPD-1/PD-L1 interaction and decrease immunosuppressive signalling in exhausted T cells (16). In cancer therapy methods, overexpression of sPD-1 as an adjuvant along with cancer vaccines (17) and secretion of sPD-1 from oncolytic virus-infected cells in TME (18) could enhance the proliferation and immunological cytotoxicity of T cells against PD-L1<sup>+</sup> tumor cells.

In recent years, CRISPR/Cas9 technology is the most practical advancement in biotechnology to manipulate the genome with high accuracy. CRISPR/Cas9 systems have been applied in several studies for genetic editing of lymphocytes. A disruption in the *PDCDI* gene sequence through the non-homologous end joining (NHEJ) approach of CRISPR/Cas9 to knock-out PD-1 expression is a new therapeutic strategy that has been used in chimeric antigen receptor (CAR)-T cell therapy and tumor infiltrated lymphocytes (TILs) therapy. The intention of this strategy is to promote an immune system response and eliminate tumor cells (10, 11, 19). Some of these developed CRISPR-engineered T cells are in clinical trial phase 1 studies (20).

Based on recent studies using sPD-1 to improve the functionality of the T cells, besides the positive effect of blocking mPD-1 expression by the CRISPR/Cas9 system, we hypothesize that deletion of exon-3 (transmembrane domain) from the *PDCDI* gene of the T cells could interrupt full-length mPD-1 expression and increase sPD-1 production to overcome exhaustion. The exon-2 sequence was considered a target location for manipulating the *PDCDI* gene to block all transcripts of the PD-1 protein in recent studies. We intend to keep both exon-1 and exon-2 intact to have an IgV-like domain and skip exon-3 of PD-1 mRNA to delete the transmembrane domain in this protein sequence.

We used the CRISPR/Cas9 system in this study because

of the promising results of this system for targeted exon skipping. The CRISPR/Cas9 studies show two approaches for exon skipping. The first approach is to design sgRNAs for the splicing sites to create random insertion and deletion (indel) mutations at the specified intron-exon edge and remove the exon at the splicing level through selective alternative splicing. The second approach is to design two sgRNAs for the upstream and downstream regions of the specified exon, which could ultimately lead to the deletion of the exon at the genome level (21-23). Here, we designed two sgRNAs for the upstream and downstream sequences of exon-3 in the *PDCDI* gene. At least one sgRNA targeted the splicing site to change the structure of the expressed protein from the membrane to the soluble form by skipping the target exon and remove the transmembrane domain of PD-1. Finally, we investigated the effect of secreted sPD-1 from pooled engineered and non-engineered T cell supernatant on survival and proliferation of lymphocytes in the TME.

## Materials and Methods

### Soluble PD-1 protein in the in-silico laboratory

In this experimental study, bioinformatic tools were used to compare the mPD-1 and sPD-1 protein structures and their locations in the cells. The location of the PD-1 protein before and after exon-3 deletion in CELLO v.2.5 and LocTree v.3, the protein subcellular localization prediction web servers, were compared (Tables S1-S4, See Supplementary Online Information at [www.celljournal.org](http://www.celljournal.org)). Prediction of membrane helices and a plot of the protein sequence with TMHMM Server v.2.0 confirmed the removal of transmembrane helices in exon-3 deleted PD-1 protein (Figs.S1, S2, See Supplementary Online Information at [www.celljournal.org](http://www.celljournal.org)). CD-search online software from the NCBI database was used to predict the conserved domains in the mPD-1 and sPD-1 proteins. IgV-PD1, a functional domain from the Ig superfamily, was detected in both natural (mPD-1) and exon-3 deleted PD-1 (sPD-1) proteins, and this indicated the functionality of these proteins (Figs.S3, S4, See Supplementary Online Information at [www.celljournal.org](http://www.celljournal.org)).

### Prediction of splicing sites, sgRNA design, and dual cloning

Prediction of splicing regions in intron 2-3/exon-3 edge and exon-3/ intron 3-4 edge was done through NetGene2 Server v.2.42 based on a neural network prediction algorithm to determine target regions to design the sgRNAs (Table S5, See Supplementary Online Information at [www.celljournal.org](http://www.celljournal.org)).

CHOPCHOP v.3.0.0 ([chopchop.cbu.uib.no](http://chopchop.cbu.uib.no)) (24) and CRISPOR v.5.01 ([crispor.tefor.net](http://crispor.tefor.net)) (25) tools were used to design the sgRNAs. The closest protospacer adjacent motif (PAM) to the splicing regions in the upstream and downstream introns (intron 2-3 and intron 3-4) of exon-3 were defined. The best sgRNA sequences with the highest specificity and efficiency scores and low off-targets were

candidate. The final selected sgRNA sequences for this study were 5'CTGGAAGGGCACAAAGGTCA3' (right sgRNA) and 5'TTAGTCCAGGGGCCTTCATC3' (left sgRNA). Tables S6-S8 (See Supplementary Online Information at [www.celljournal.org](http://www.celljournal.org)) provides information about the sgRNAs.

We intended to transfer the CRISPR/Cas9 structure to lymphocytes. Therefore, we selected a lentiviral vector to improve the transduction result. Sense and antisense sequences of sgRNAs with the BsmBI restriction enzyme (RE) sites for cloning into the lentiCRISPRv2 puro vector (Addgene; #98290) were synthesised by Metabion AG, Germany. Each sgRNA was separately cloned into the lentiCRISPRv2 puro vector construct by digestion with BsmBI Fast Digest enzyme (Esp3I RE, Thermo Scientific™, USA, cat no: FD0454) and ligation with a T4 ligase enzyme (Thermo Scientific™, USA, catno: EL0014). In order to produce the dual sgRNAs/lentiCRISPRv2 puro vector, we first performed PCR using forward and reverse primers (5'TTTCTAGAGAGGGCCTATTTCCA3' and 5'TTCAAGACCTAGCTAGCGAATTC3'), which included cutting regions for XbaI and NheI enzymes, respectively, to target the beginning and end of the right sgRNA construct and propagate the U6 promoter, right sgRNA, and its scaffold. Next, the PCR product was cleaned with an EZ-10 Spin Column PCR Product Purification Kit (Bio Basic, Inc., Canada, cat no: BS363), then double digested with NheI enzyme (Thermo Scientific™, USA, cat no: FD0684) and XbaI enzyme (Thermo Scientific™, USA, cat no: FD0974). Finally, the lentiCRISPRv2 puro vector that included left sgRNA was restricted with NheI enzyme and subcloned by ligation of the double-digested PCR product using T4 ligase enzyme. The final cloned dual sgRNAs/lentiCRISPRv2 puro vector sequence was confirmed by forward and reverse Sanger sequencing of the right and left sgRNA sequences.

## Cell culture

The HEK293T cell line was cultured for transfection of the viral vectors to produce lentiviral particles with DMEM complete medium that included 10% FBS and 1X Pen/Strep (all from Gibco™, USA) in a 5% CO<sub>2</sub> incubator at 37°C and 95% humidity.

The Jurkat cell line (CD4<sup>+</sup> T cells) is a suitable cell line for immuno-oncology research. This cell line could be used as the exhausted T cells with PD-1 protein expression after activation. We used the Jurkat T cells for transduction of the lentiviral particles and manipulation of the *PDCD1* gene by the CRISPR/Cas9 system. The Jurkat cells were cultured in RPMI complete medium (Gibco™, USA) that included 10% FBS and 1X Pen/Strep at 37°C with 95% humidity in a 5% CO<sub>2</sub> incubator.

We used the MDA-MB-231 (PD-L<sup>+</sup>) cell line for the co-culture tests in DMEM medium. All of the cell lines were purchased from the Cell Bank at Pasteur Institute of Iran.

Renal carcinoma cells (RCC) were extracted from a patient's renal tumor tissue after filtering through a cell

strainer without digestion. The filtered cells were washed twice with PBS and cultured in RPMI medium with 15% FBS and 1X Pen/Strep in a 5% CO<sub>2</sub> incubator with 37°C and 95% humidity for 72 hours. The suspended cells were removed by washing with sterile PBS, and the adherent cells were cultured in fresh RPMI medium that included 10% FBS and 1X Pen/Strep for one week to enable the cells to reach 90% confluency. Ethical certification for the use of the patient's primary cells is provided in the Ethical Consideration section.

## Lentiviral packaging, titration, transduction, and activation

We seeded 3.8×10<sup>6</sup> HEK-293T cells on a 10 cm plate (SPL, Korea) in DMEM complete medium. After 24 hours, the supernatant of the cells was completely removed and the medium was replaced by DMEM that included 2% FBS without antibiotics, and again incubated for 2 hours. We mixed 1:2:3 ratios of the lentiviral vectors in Opti-MEM media (Gibco™), which equalled 15 µg dual sgRNAs/lentiCRISPRv2 puro (Addgene #98290), 10 µg psPAX2 (Addgene #12260), and 5 µg pMD2G (Addgene #12259) vectors, respectively. Next, 1 mg/mL of branched polyethyleneimine (PEI) transfection reagent (Sigma-Aldrich, USA) was combined with the vector mixture in a 1:2 (PEI: vector) ratio in Opti-MEM media and incubated for 20 minutes at room temperature (RT). Finally, the transfection mix was transferred to the HEK-293T cells. After an 18-hour incubation, the media was replaced by DMEM complete medium. The supernatant that included the lentiviral particles was harvested at 72 hours post-transfection and centrifuged for 10 minutes at 2000×g to pellet any packaging cells; then, the supernatant was filtered through a 0.45 µm polyethersulfone (PES) filter (Jet Bio-Filtration Co., Ltd., China). Finally, the lentiviral particles were concentrated with polyethylene glycol (PEG) 6000 (Sigma-Aldrich, USA) and NaCl. The concentrated viral particles were aliquoted in PBS and stored at -80°C.

In order to indicate the viral particle titration, the viral RNA was extracted with a BehPrep Viral RNA Extraction Kit (BehGene Biotech Co., Iran). cDNA synthesis was done using a RT-ROSET Kit (ROJE Technologies Co., Iran). A pair of primers that targeted the LTR region of the lentiCRISPRv2 puro vector was designed to titrate the produced lentiviral particles by standard quantitative polymerase chain reaction (qPCR). The primer sequences were 5'TGTGTGCCCGTCTGTTGTGT3' (forward) and 5'GAGTCCTGCGTCGAGAGAGC3' (reverse).

A total of 5×10<sup>5</sup> Jurkat cells were seeded per well in a 24-well plate (SPL, Korea) and transduced with dual sgRNAs/CRISPR lentiviral particles at Multiplicity of infection (MOI) of ten diluted in RPMI medium with 5% FBS and 8 µg/mL polybrene (Sigma-Aldrich). The polybrene concentration for transduction was determined by the MTT assay results (data not shown). The transduction mixture was incubated for 20 minutes at RT, then the plate was centrifuged at 800 ×g for 90 minutes



at 32°C according to the spinoculation protocol (26). The media was replaced at 24 hours post-transduction, and the plate was incubated again. After 24 hours, 50 ng/mL PMA and 1 µg/mL PHA were added to the media to enable cell activation. At 96 hours post-transduction the Jurkat cell population of active transduced and non-transduced cells (engineered and non-engineered cells) were collected and called the pooled cell group. The positive control cell group consisted of 5×10<sup>5</sup> Jurkat cells seeded per well in a 24-well plate that was activated with PMA and PHA for 48 hours. Jurkat cells without transduction and activation were cultured as negative control cell group. The cells and their supernatants from the pooled and control groups were collected separately for subsequent analysis.

### Analysis of extracted DNA

DNA from the pooled cells and negative control groups were extracted using a DNA Extraction Kit (Gene Transfer Pioneers Co., Iran). A forward primer targeting intron 2-3 upstream of exon-3 and reverse primer targeting intron 4-5 downstream of exon-3 with the primer sequences of 5'TCTGTCTCTAGCTCTGGAAGC3' and 5'AGAATGTGAGTCCTGCA3', respectively, were used for PCR. The PCR was done with Taq DNA Polymerase 2x Master Mix, 1.5 mM MgCl<sub>2</sub> (Ampliqon, Denmark) by the standard program and at 58°C for annealing of the primers. The PCR products were sequenced by Pishgam Co., Iran. Sanger sequencing data from the PCR products of the pooled cells and control groups were analysed with Chromas Lite v.2.5 by focusing on nucleotide peaks in the sequencing chromatogram. Alignment was done between the pooled cells group and the control group sequencing data with CLC DNA Workbench v.6 in order to survey indel mutation in the targeting locations of the sgRNAs. In addition, tracking of indels by decomposition (TIDE) (<https://tide.nki.nl>) tool v.3.3.0 (27) and interference of CRISPR edits (ICE) (<https://ice.synthego.com>) tool v.3.0 from Synthego were used for Sanger sequencing data analysis. The purpose of decomposing and aligning based on the TIDE and ICE tools was a visualisation of the indel spectrums and estimation of the overall editing efficiency from the sequencing data of the pooled cells in the comparison control group.

### Analysis of synthesised cDNA

RNA from the pooled cells group and the positive control group were extracted using a SanPrep Column MicroRNA Mini-Prep Kit (Bio Basic, Inc. Canada). cDNA synthesis was carried out with the RT-ROSET Kit (ROJE Technologies Co., Iran) protocol. The reverse PCR was designed to check the exon-3 deletion in the PD-1 mRNAs. The forward primer for targeting exon-2 was 5'CTTCCGTGTCACACAAGTGC3' and reverse primer for targeting exon-4 was 5'GAGGGGTCCTCCTTCAGG3'. The PCR was performed with Taq DNA Polymerase 2x Master Mix at 58°C to anneal the primers by a standard program. The size of the PCR product band on 3% gel agarose in the presence and absence of exon-3 must be

360 bp and 204 bp, respectively.

Real-time polymerase chain reaction PCR (RT-PCR) was used to investigate the PD-1 expression pattern in mRNA from the pooled cell group and compare them with the positive control group. The control primers 5'CTTAGACTCCCCAGACAGG3' (forward) and 5'GATGTGTTGGAGAAGCTGC3' (reverse) were used for targeting upstream exons located at the junction of exon 1-2 and exon 2, which were continually expressed in the mPD-1 and sPD-1 transcripts. Test primers [5'TGCTGCTAGTCTGGGTCCT3' (forward) and 5'GAGGGGTCCTCCTTCAGG3' (reverse)] were used to target exon-3 and the exon 4-5 junction, which were continually expressed in the mPD-1 transcript and had reduced expression in the sPD-1 transcript. The relative expression calculation from the RT-PCR results enabled us to determine the change in PD-1 expression pattern. RT-PCR was performed using with RealQ Plus Master Mix Green High ROX™ (Ampliqon, Denmark) at 58°C for annealing of the primers through a standard program.

### Co-culture conditions

The PBMCs were separated from healthy donor blood by Ficol-Lymphodex (Innotrain, Germany) and labelled with 5 µM carboxyfluorescein succinimidyl ester (CFSE, Sigma-Aldrich) for 10 minutes at 37°C in PBS. Labelling was stopped by the addition of a 10-fold volume of PBS and the PBMCs were subsequently washed for three times in PBS. The labelled cells were placed in a 24-well plate in RPMI complete medium to incubate for 10 hours. The next day, the suspended cells were collected as CFSE-labelled lymphocytes for co-culture.

RCC and MDA-MB-231 cancer cells, as PD-L<sup>+</sup> cells, were seeded in 24-well plates to achieve 50% confluency. Then, the CFSE-labelled lymphocytes were added to each well for co-culture with the cancer cells. The effector to target cell ratio was determined as 10:1. A total of 150 µl of supernatant from the pooled cell group (collected from the transduction step) was added to the medium of the cells according to the panels in Table 1. After 72 hours, the suspended and adherent cells were collected for the proliferation and apoptosis assays by flow cytometry.

### Flow cytometry assay

Flow cytometry was performed using the FITC anti-human CD279 (PD-1) antibody (Sina Biotech Co., Iran) for analysis of mPD-1 expression on the surfaces of the pooled cells, and the positive and negative controls.

The proliferation assay was done with APC anti-human CD3 antibody (OKT-3, Elabscience, USA) and CFSE label for positive gating of lymphocytes by flow cytometry.

The collected cells were prepared with an Annexin V-FITC/7-AAD Kit (Elabscience, USA) according to the manufacturer's protocol for the apoptosis assay. The flow cytometry results were analysed by FlowJo™ software v.10.

**Table 1:** Co-culture states for the intended assays

Co-culture panels	Co-culture conditions	Assay
Lymphocyte panel	Lymphocyte CFSE-label	Negative control for proliferation assay
	Lymphocyte CFSE-label culture with PHA and PMA	Positive control for proliferation assay
	Lymphocyte CFSE-label culture with supernatant of pooled cell group	Proliferation assay
RCC panel	Lymphocyte CFSE-label co-culture with RCC	Proliferation and apoptosis assays
	Lymphocyte CFSE-label co-culture with RCC and supernatant of pooled cell group	Proliferation and apoptosis assays
MDA-MB-231 cell line panel	Lymphocyte CFSE-label co-culture with MDA-MB-231 cell line	Apoptosis assay
	Lymphocyte CFSE-label co-culture with MDA-MB-231 and supernatant of pooled cell group	Apoptosis assay

RCC; Renal carcinoma cells and CFSE: Carboxyfluorescein succinimidyl ester.

### Dot blot assay

A total of 4  $\mu$ l of the cell supernatants were spotted on the PVDF strip for the dot blot assay. The detection procedure was done with biotinylated anti-human PD-1 antibody (Sina Biotech Co., Iran), streptavidin-POD (Sigma-Aldrich), and a DAB substrate (Roche, USA), respectively. Intensity of the brown spots were captured and quantified with ImageJ v.2 software.

### Statistical analysis

Statistical analysis was performed using Prism 9 software (GraphPad Software, LLC, USA).  $P < 0.05$  indicated statistical significance.

### Ethical consideration

The Vice Chancellor of Research Affairs, Tehran University of Medical Sciences, Tehran, Iran approved the acquisition of the primary cell culture in this study (IR.TUMS.VCR.REC.1397.524).

### Results

#### Cloning, viral packaging, and dual sgRNAs/CRISPR lentiviral particles transduction

Figure 1A shows successful cloning of the sgRNAs into the lentiCRISPRv2 puro and sub-cloning of the right sgRNA construct (U6 promoter, sgRNA, and scaffold) into the lentiCRISPRv2 puro vector, including the left sgRNA. Both forward and reverse Sanger sequencing confirmed the accuracy of the dual sgRNAs/lentiCRISPRv2 puro vector sequence (results not shown).

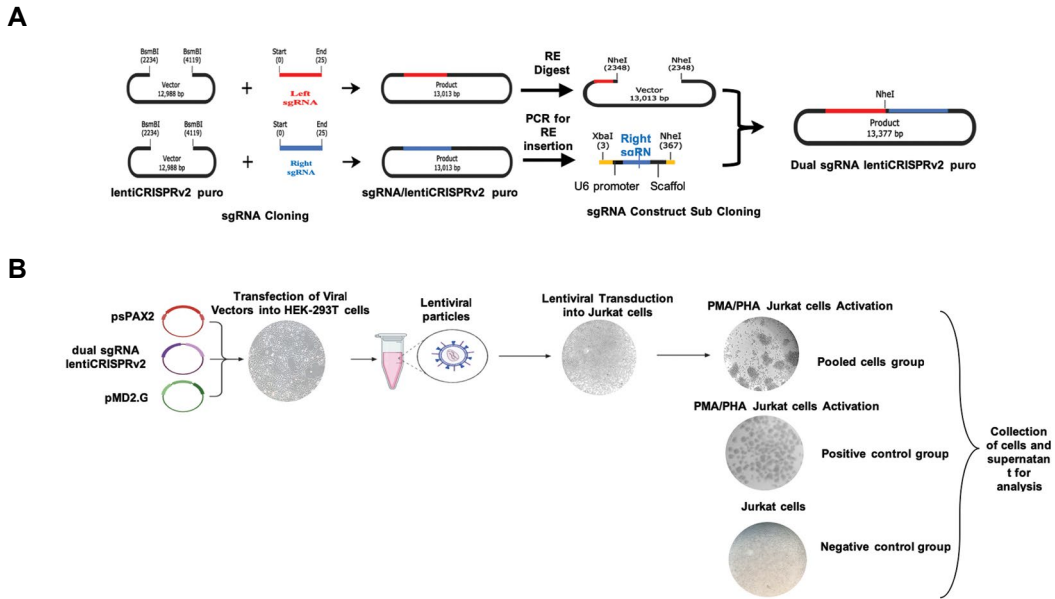
We transfected the viral vectors (lentiCRISPRv2 puro, psPAX2, pMD2.G) into the HEK-293T cell line and the packaging processes were done. qPCR titration results showed that there were  $22 \times 10^6$  RNA copy number/mL of collected dual sgRNAs/CRISPR lentiviral particles after

concentration with PEG 6000. The lentiviral particles with MOI of 10 were transduced to the Jurkat cell line. We noted that 96 hours after viral transduction and PMA/PHA activation, the Jurkat cells formed clumps with less than 50% viability because of the activation procedure effect (Fig.1B). The experimental groups are also shown in Figure 1B.

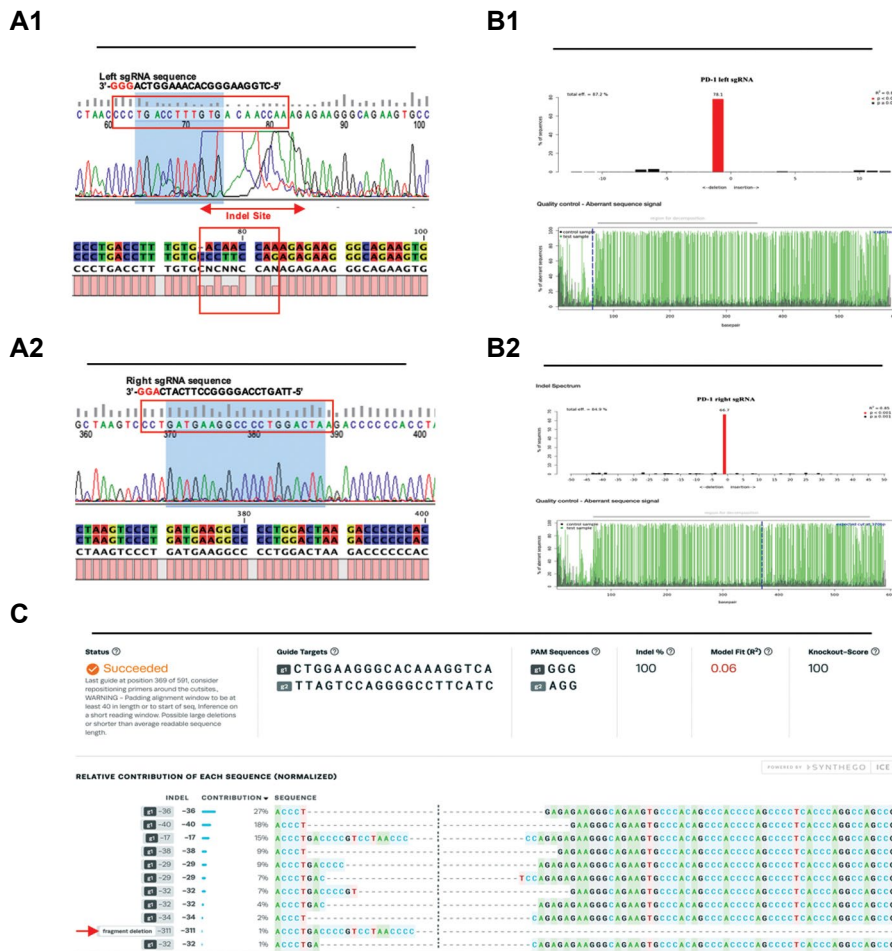
#### Sanger sequencing data analysis confirmed indels in the pooled genome

Figure 2A1 shows the changes in nucleotide peaks of the DNA sequencing chromatogram of the pooled cells compared to control cells. There were noises near the double strand break (DSB) region of the left sgRNA targeting location in the *PDCDI* gene, which indicated indel in the specified location. The alignment results between the pooled and control group sequences near the DSB regions of the left sgRNA confirmed changes in several nucleotides (Fig.2A1). However, we did not detect any nucleotide changes in the chromatogram signal plot and alignment result in the right sgRNA (Fig.2A2).

Sanger sequencing data analysis in TIDE separately for each sgRNA estimated that the overall editing efficiency for the left and right sgRNAs were 87.2 and 84.9% with  $R^2$  model fit of 0.87 and 0.85 in order. The TIDE tool results showed that 78% of the pooled cells had one nucleotide deletion in charge of the left sgRNA and 66% in the right sgRNA ( $P < 0.001$ , Fig.2B1, B2). The ICE tool was used to simultaneously check the two sgRNA. ICE results showed 100% indel efficiency with 0.06  $R^2$  model fit. We noted that 99% of the indels occurred through the contribution of the left sgRNA; their indel sites were in the edge of the intron 2-3/exon-3 splicing region. One percent of the pooled cells were estimated that have large deletions, 311bp, which could be referred to as exon-3 deletion at the genome level with the simultaneous contribution of left and right sgRNAs (Fig.2C).



**Fig.1:** From cloning to lentiviral particle production processes are depicted. **A.** Cloning of the dual sgRNAs construct in the lentiCRISPRv2 puro vector. First, each sgRNA is cloned into the lentiCRISPRv2 puro vector, then the right sgRNA construct with a U6 promoter and its scaffold is cloned into the left sgRNA lentiCRISPRv2 puro vector with the XbaI/NheI RE sites. **B.** Production of the lentiviral particles and transduction pathway. Transfection of plasmids into HEK-293T for lentiviral packaging, transduction into the Jurkat cell line, and activation process for the pooled cell and control groups are shown.



**Fig.2:** Sanger sequencing data analysis are reported the changes in target sequence. **A1.** Chromatogram plot of left sgRNA and alignment result determines the nucleotide changes in the target region. **A2.** The chromatogram plot and alignment result of the right sgRNA does not show any detectable signs. **B1, B2.** Tracking of indels by decomposition (TIDE) analysis plot of each sgRNA separately with total efficiency of 78.2% for the left and 84.9% for the right sgRNA. **C.** Simultaneous interference of CRISPR edits (ICE) analysis of dual sgRNAs with 100% efficiency. The arrow indicates a large fragment deletion in the pooled cells that could be referred to as an exon-3 deletion at the genome level.



### Changes in expression pattern of the PD-1 transcripts in pooled mRNA

Reverse PCR was performed to confirm the exon-3 deletion at the mRNA level in the pooled cell group compared to the positive control group. Figure 3A1 shows the designed primers for reverse PCR, and the band sizes in the presence and absence of exon-3 are shown. The PCR product of the positive control group had only a 360 bp band on 3% agarose gel. The PCR product of the pooled group had 360 bp and 204 bp bands that referred to the mPD-1 and sPD-1 transcripts, respectively (Fig.3A2).

Two primer pairs were used for RT-PCR to investigate the change in PD-1 expression pattern. Figure 3B1 shows the control primer and test primer pairs, and their target sites. According to the results obtained from RT-PCR and their relative expression calculation, it was determined that the mPD-1 expression decreased by 50% in the pooled cells compared to the positive control group (Fig.3B2).

### Reduction of membrane PD-1 expression versus increased soluble PD-1 in pooled cells using CRISPR/Cas9

Flow cytometry was performed using FITC anti-human

PD-1 antibody to investigate the expression level of mPD-1 on the surfaces of the pooled cells and control groups. Only 5% of Jurkat cells expressed mPD-1 in the negative control group. However, 70.91% of the cells expressed mPD-1 after activation of Jurkat cells in the positive group. The pooled group, after transduction and activation of Jurkat cells, only 58.33% of the cells were mPD-1 positive. There was a 12.85% reduction in mPD-1 positive cells after manipulation. Figure 4A1, A2 show the flow cytometry results and related diagram of the percentage of Jurkat cells that expressed mPD-1.

Biotinylated anti-human PD-1 antibody was used in a dot blot to check sPD-1 protein expression in the supernatant of the pooled cells group compared to the control positive and negative groups. Brown dots were observed with the pooled group and control positive supernatants. Therefore, both groups had different intensities of sPD-1 expression (Fig.4B1). The captured image of the dot blot strip was quantified using ImageJ software. The results showed that the increased level of soluble protein expression in the supernatant was 9.7%, from 28.26% for the control positive group to 37.96% for the pooled cells group (Fig.4B2).

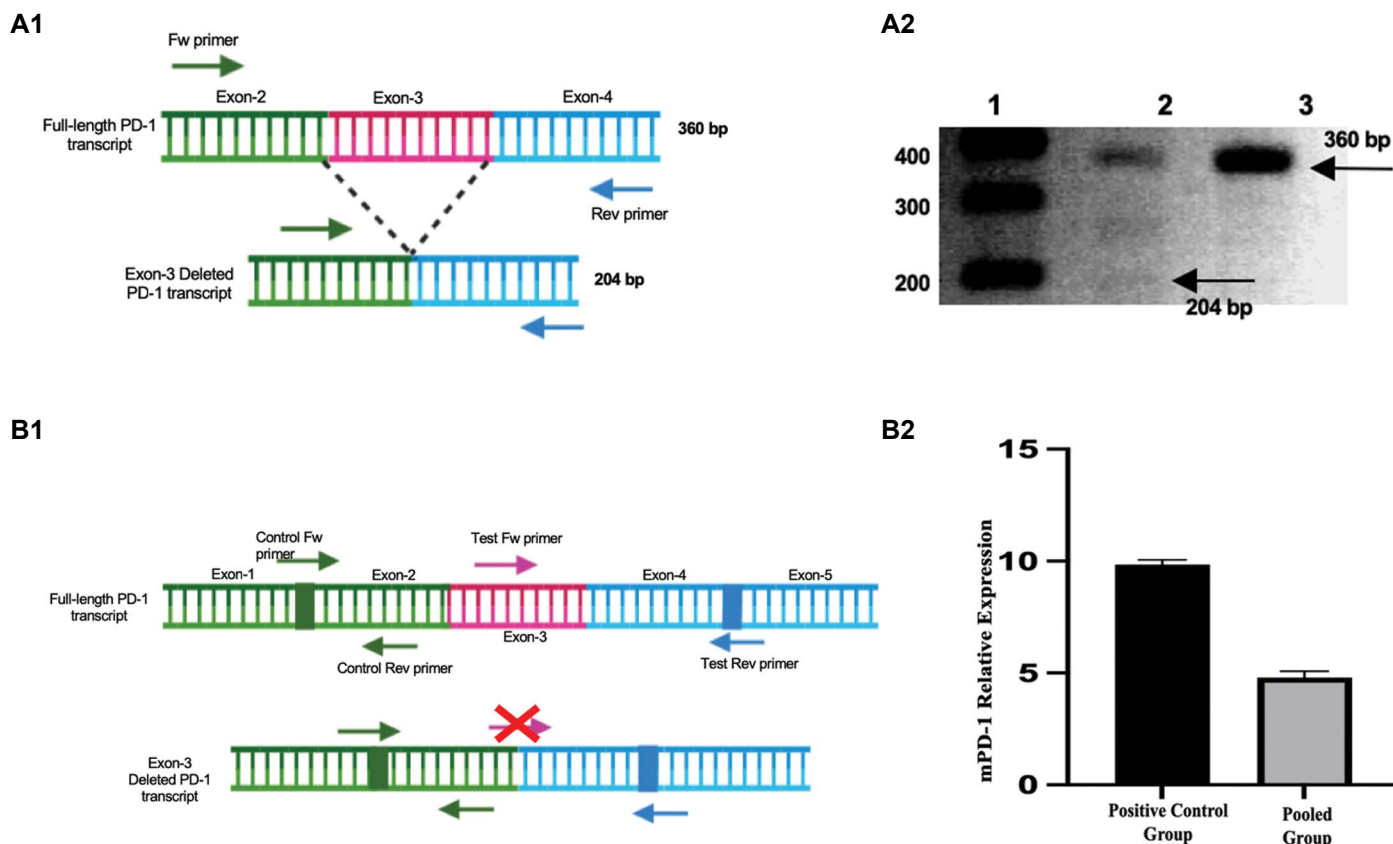


**Fig.3:** PD-1 transcript expression patterns are analysed. **A1.** Full-length and exon-3 deletion PD-1 transcripts are shown. A pair of primers for reverse-PCR upstream (exon-2) and downstream (exon-4) of exon-3 are depicted. **A2.** The result of the reverse PCR product was run on 3% agarose gel electrophoresis. Lane 1: 100 bp DNA ladder (Yekta Tajhiz Azma, Iran), lane 2: PCR product of the pooled cells group, and lane 3: PCR product of the positive control group. Arrows show the 360 bp and 240 bp bands. The middle band is an unwanted band that also appeared in the control. **B1.** Schematic picture of real-time PCR (RT-PCR) with two primer sets. Control primers target upstream exons of PD-1 mRNA with stable expression for membrane PD-1 and soluble PD-1. The test primers target exon-3 of PD-1 mRNA for checking the membrane PD-1 reduction after exon deletion. **B2.** Results of RT-PCR with two sets of primers for the positive control and pooled cells, analysed with relative expression calculation in Prism with two sample sizes and  $P=0.0024$ . PCR; polymerase chain reaction.

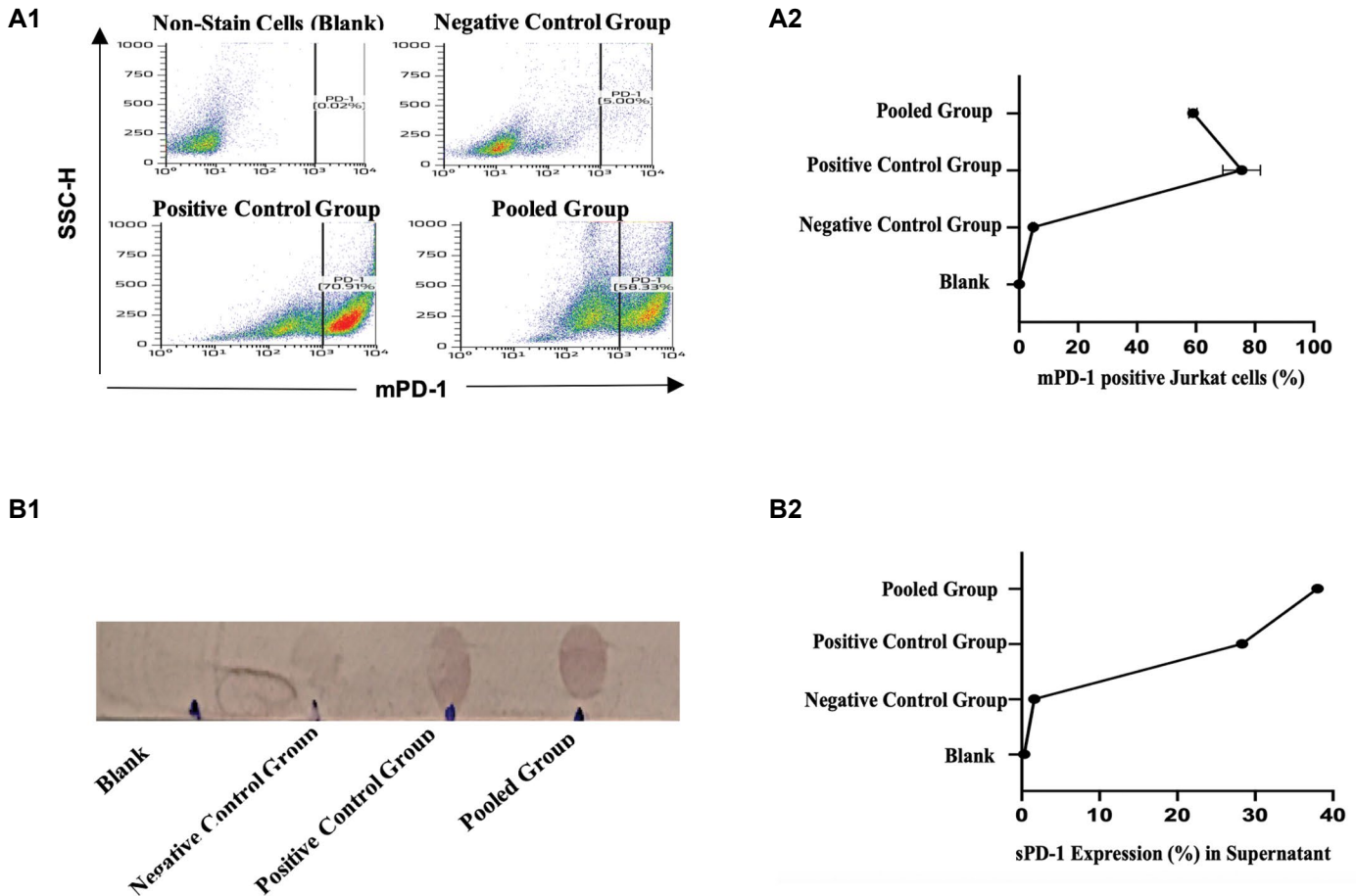


**Fig.4:** Effect of dual sgRNAs/CRISPR lentiviral particles on PD-1 protein expression in Jurkat cells versus control groups are reported. **A1.** Flow cytometry results for four groups stained with FITC-anti-PD-1 antibody. **A2.** The percentage of membrane PD-1 (mPD-1) positive Jurkat cells derived from flow cytometry results, with two sample sizes and  $P < 0.0001$ . **B1.** Strip image of dot blot assay for detection of soluble PD-1 (sPD-1) in the supernatant. **B2.** The dots on the strip were quantified with ImageJ software. The results are reported as percentages.

### Lymphocyte proliferation and apoptosis assay in the co-cultures

The selection of candidate cancer cells was based on surface PD-L1 protein expression. It has been reported that the MDA-MB-231 breast cancer cell line has a high expression level of PD-L1. RCC was selected as a primary cancer cell that expresses PD-L1. High expression level of PD-L1 in these cells was confirmed by qPCR (data not shown).

We sought to examine the effect of sPD-1 in the supernatant of the pooled cells group on the proliferation and apoptosis of lymphocytes, alone and in co-culture with PD-L1<sup>+</sup> cancer cells. Therefore, we designed co-culture panel tests (Table 1) that had an effector to target cell ratio of 10:1. CFSE-labelled lymphocytes were collected after 72 hours of co-culture with or without RCC. Supernatant from the pooled cells group was assessed by flow cytometry to evaluate CD3-CFSE<sup>+</sup> gated cell proliferation. The proliferation histograms were analysed with FlowJo™ v.10 software. CFSE-labelled lymphocytes were considered to be the negative control and non-stained lymphocytes comprised the blank that did not have any proliferation peaks in the histogram. The histogram of

PHA/PMA activated CFSE-labelled lymphocytes was the positive control for proliferation, which separated into divided peaks of proliferated cells and an undivided peak of non-proliferated cells. Histograms of other co-culture groups were compared with the positive and negative control histograms (Fig.5A1). The percentage of proliferated lymphocytes or cells with lower CFSE in the divided peaks of each condition is shown in Figure 5A2. In lymphocytes co-cultured with RCC, we observed that ~37% of cells were proliferated; in the co-culture of lymphocytes and supernatant, this rate was ~45%. In the lymphocyte, RCC, and supernatant co-culture, the proliferated CD3-CFSE<sup>+</sup> lymphocytes increased to ~55%. The supernatant, including sPD-1, had a positive effect on lymphocyte proliferation with or without tumor cells (Fig.5A2).

We tested apoptosis of the CFSE<sup>+</sup> gated lymphocytes by flow cytometry and an Annexin V-FITC/7-AAD kit. In the first step, the cells were gated by CFSE positivity. Then, these cells were defined by 7-AAD and Annexin V-FITC. The percentage of late and early apoptosis (Q2: Annexin V positive and 7-AAD positive and Q3: Annexin V positive and 7-AAD negative, respectively)



after CFSE<sup>+</sup> gating of lymphocytes co-cultured with RCC was 13.36%. The apoptosis percentage of CFSE<sup>+</sup> lymphocytes co-cultured with RCC and supernatant was 3.3%. There was a 10% reduction in the percentage of lymphocytes that underwent apoptosis after the addition of supernatant to the co-culture. There were 12.5% more viable lymphocytes in the presence of supernatant than viable lymphocytes co-cultured with only RCC. This positive function on lymphocytes could be attributed to the influence of sPD-1 in the supernatant. Figure 5B1 shows the percentages of lymphocytes (live, necrotic, late apoptosis, and early apoptosis). The percent of

surviving CFSE<sup>+</sup> gated lymphocytes co-cultured with the MDA-MB-231 cell line in the presence and absence of supernatant had a 14.8% difference (Fig.5B2). The percentages of lymphocytes (live, necrosis, late apoptosis, and early apoptosis) in the different co-culture conditions are shown in Figure 5B2.

Microscopic cell images of the co-culture conditions confirmed the proliferation and apoptosis results of the lymphocytes. Furthermore, we observed morphological changes indicative of apoptosis in the tumor cells in the presence of supernatant (Fig.5C).

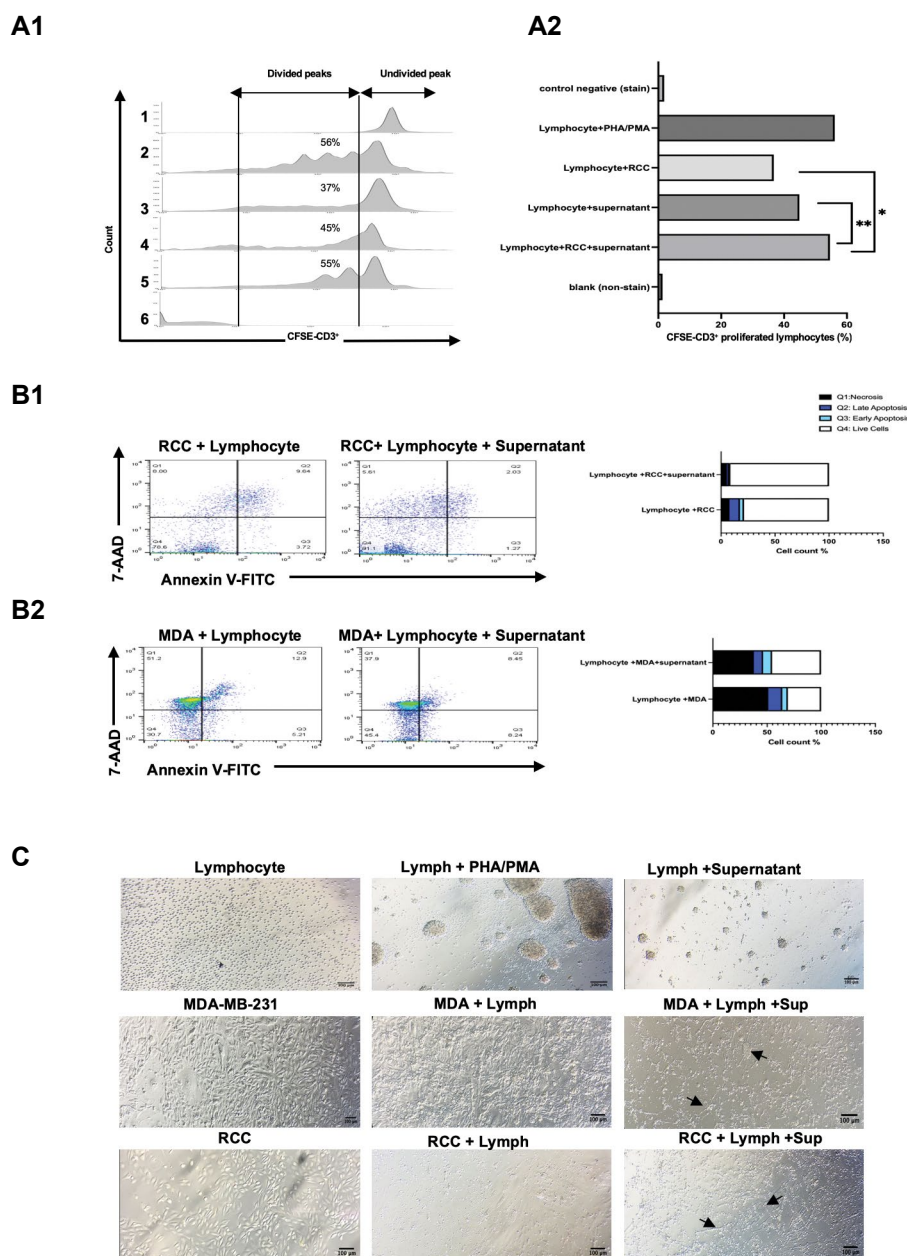


**Fig.5:** Effect of sPD-1 in supernatant on proliferation and apoptosis of lymphocytes are reported. **A1.** Histogram plot for proliferation of CD3-CFSE<sup>+</sup> gated cells. 1; Negative control (CFSE-labelled lymphocytes), 2; Positive control (CFSE-labelled lymphocytes activated with PHA/PMA), 3; CFSE-CD3<sup>+</sup> gated lymphocytes co-cultured with renal carcinoma cells (RCC), 4; CFSE-CD3<sup>+</sup> gated lymphocytes co-cultured with supernatant, 5; CFSE-CD3<sup>+</sup> gated lymphocytes co-cultured with RCC and supernatant, and 6; Blank (unstained lymphocytes). **A2.** Percentage of proliferated cells. \*; ~18% difference, \*\*; ~9.5% difference). **B1, B2.** Apoptosis assay for the CFSE<sup>+</sup> gated cells. Co-culture states are shown. Four states for the cells are shown in the diagram (live, late apoptosis, early apoptosis, and necrosis). **C.** Cell images (scale bar: 100 μm, magnification: 10x). Arrows show the changes in cancer cell morphology. CFSE; Carboxyfluorescein succinimidyl ester and RCC; Renal carcinoma cell.

## Discussion

In general, the infiltrated T-cells in the heterogeneous tumor cell population are classified into different levels of functionality. Cell-intrinsic processes, such as the negative signalling pathway of immune checkpoint inhibitors (ICIs), and cell-extrinsic factors, such as immunosuppressive factors in TME, cause a reduction in T cell function and lead to exhaustion. Interventional treatments that include immune checkpoint blockade (ICB) therapy could be effective in restoring exhausted T cell activity. Interruption of the PD-1/PD-L1 negative signalling pathway via designed monoclonal antibodies showed better responses in comparison with other antibodies against inhibitory receptors, such as CTLA4 and TIM3 (28, 29). We took into consideration the latest studies of PD-1 and, in this experiment, targeted the pattern of PD-1 molecule expression in T cells that affected the PD-1/PD-L1 signalling pathway. Our approach used knocked-out mPD-1 versus increasing sPD-1 expression. Then, we used a dual sgRNAs/CRISPR system to skip exon-3 in the *PDCDI* gene of Jurkat T cells. Our results from DNA sequencing data of the pooled cells (population of transduced and non-transduced T cells) confirmed the deletion of exon-3 from *PDCDI* gene in parts of the cell population. A reduction in the mPD-1 transcript in the pooled cells was confirmed by flow cytometry and RT-PCR. Increased sPD-1 expression in the supernatant of pooled Jurkat cells was another outcome of this study. The co-culture conditions that included the supernatant of pooled cells confirmed the effect of sPD-1 on boosting lymphocyte proliferation and reducing their apoptosis.

Aside from CD8<sup>+</sup> T cells, tumor antigen-specific CD4<sup>+</sup> T cells that have an anti-tumor function also accumulate in the tumor environment. These CD4<sup>+</sup> T cells have similar exhaustion patterns due to the high expression level of inhibitory receptors. Studies show that the scRNA-Seq panel of the CD4<sup>+</sup> TILs and its phenotype analyses are parallel to CD8<sup>+</sup> TILs; therefore, the exhaustion process and related hallmarks are similar (30). The phenotypes of exhausted T cells are not homogeneous, and this lack of homogeneity is observed in both CD8<sup>+</sup> and CD4<sup>+</sup> T cells. PD-1 expression, as the first inhibitory marker, is the important point in these cells. Therefore, the use of anti-PD-1/PD-L1 therapies can be a front line ICB to restore T cell function, both in progenitor cells to prevent exhaustion and in terminal cells to return exhaustion (2). The Jurkat cells are immortalized human CD4<sup>+</sup> T lymphocyte cells that can be a model for exhaustion research because of the importance of CD4<sup>+</sup> T cells in the exhaustion process and the importance of blocking and changing PD-1 expression in these cells. The Jurkat cell line has been used in several studies for genetic engineering purposes, including studies of the interactions between PD-1 and PD-L1 (31, 32). Our flow cytometry results showed stimulation of mPD-1 expression after PMA/PHA activation of Jurkat cells. Therefore, we chose this cell line for genomic editing of the *PDCDI* gene sequence.

The PD-1 molecule has a soluble form that is translated

after alternative splicing in addition to the membrane form responsible for binding to its ligands on the surface of cancer cells. Among four splice variants of PD-1 mRNA, the exon-3 deleted variant expresses a soluble transcript variant. The sPD-1 variant tends to bind PD-L1 through its IgV-like domain and compete with mPD-1. sPD-1 could block the negative signalling pathway of mPD-1/PD-L1 to reduce apoptotic death of tumor-specific T cells and increase their survival and proliferation (16, 33). The inhibitory function of sPD-1 molecule in TME is similar to anti-PD-L1 monoclonal antibody functions (7, 34). The therapeutic value of the sPD-1 molecule in combination with cancer peptide vaccines and CAR-T cells, as an adjuvant, has been proven to improve the quality of cancer immunotherapy (35, 36). The structure of sPD-1 used in recent studies was the transgene construct that included exon-1 and 2 of the *PDCDI* gene that expressed in target cells, besides the natural expression of mPD-1 in lymphocytes. We used the exon skipping approach of the CRISPR/Cas9 system to target the *PDCDI* gene in T cells and mimic natural alternative splicing by removing exon-3 and changing the protein expression pattern permanently from its membrane to its soluble form. We observed that active Jurkat cells had baseline sPD-1 expression in their supernatant in addition to mPD-1 on their surface; after engineering of the cells and removal of *PDCDI* exon-3 with dual sgRNAs/CRISPR, the expression pattern showed increased sPD-1 and decreased mPD-1 in the pooled cells.

CRISPR gene knock-out methods used in recent studies caused disruption of the *PDCDI* gene and blocked both sPD-1 and mPD-1 expression (10-12, 19). However, in our method, mPD-1 expression was distorted and the soluble form of the *PDCDI* gene was expressed. Therefore, negative signalling and mPD-1/PD-L1 in T cells would be blocked. Total sPD-1 expressed by engineered T cells could interfere with the binding of mPD-1/PD-L1/2 and PD-L1/CD80 (B7-1), and block their inhibitory action in T cells (37).

We used a combination of two approaches for exon skipping level based on the latest studies of CRISPR/Cas9 (22). Here, we used a dual sgRNAs/CRISPR construct. The selected left sgRNA could target the splicing site and the right one could not. We expected to have an exon-3 deletion in the genome if both of the sgRNAs were functional. Conversely, we expected to have an exon-3 deletion in the mRNA transcript after splicing if only the left sgRNA was functional, and result in indels upstream of the splicing site. The results of DNA sequencing analysis from the pooled cells showed changes in the chromatogram plot sequence. TIDE analysis of the pooled cell DNA sequences did not show any exon deletion due to the limitations of the tools; however, we observed changes upstream and downstream of exon-3 at the DNA level due to both sgRNAs. The limitations of TIDE analysis are the inability to analyse two sgRNAs and the incapability to calculate indel size range greater than 50 bp which would not be able to estimate large deletions. Therefore, this

tool could not analyse large deletions in sequences, which would be expected in our pooled cell genomes. The ICE tool could simultaneously analyse both sgRNAs in the pooled manipulated cells compared to control sequences. Our results from ICE showed deletions that ranged from 17 bp to 311 bp, which confirmed changes in the genome level of the pooled cells. The low  $R^2$  model fit in the result of ICE was attributed to the indel size range limitation in this tool. Ultimately the sequencing data could confirm the indels in target sequence. In order to improve the results and show the exact change at the genome level in each cell, we should do clonal selection with puromycin. We will take this into consideration in our future study.

According to our design, exon skipping could be expected at the mRNA level based on alternative splicing of exon-3. We detected the deleted exon-3 sequences with reverse PCR in the pooled mRNA and did not detect any deletion in the positive control. RT-PCR and flow cytometry results showed a reduction in mPD-1 transcript expression in the pooled cells compared to the controls, which confirmed the change in pattern expression. Dot blot results showed an increase in sPD-1 in the pooled cells. Dot blot, as a semi-quantified method, also detected and confirmed the functionality of the sPD-1 secreted in the supernatant. Overall, there was a significant change in pattern between mPD-1 in the population of pooled cells and sPD-1 in its supernatant. A considerable point in this study was the proof of positive function of the sPD-1 protein in the collected pooled cell supernatant on proliferation and survival of CD3<sup>+</sup> lymphocytes co-cultured with PD-L1<sup>+</sup> cancer cells.

## Conclusion

The positive results obtained by using the CRISPR/Cas9 system for exon-3 skipping of the *PDCDI* gene in T cells to knock-out mPD-1 expression and increase sPD-1 in the supernatant to overcome exhaustion should be further confirmed. This experiment could be improved by the use of clonal selection, single-cell analysis, optimisation of lentiviral transduction efficiency or non-viral methods, and investigation of off-targets. Furthermore, our recommended method could engage with ACT therapies such as TILs and CAR-T cell therapy to overcome their exhaustion instead of anti-PD-1/PD-L1 antibodies or PD-1 knock-out. The advantage of this method is the ability for local treatment, which prevents the cytotoxic side effects and autoimmunity in systemic ICB therapies. This method could be generalized for other inhibitory receptors to produce soluble forms by using the CRISPR/Cas9 exon skipping strategy.

## Acknowledgments

This study was Ph.D. thesis supported by Tehran University of Medical Sciences, Tehran, Iran (grant: 97-03-87-39820). The authors gratefully acknowledge support from the Iran National Science Foundation (INSF grant: 97011707). The authors declare no conflict of interest.

## Authors' Contributions

Z.Y.-N.; Formal analysis, Investigation, Data curation, Visualisation, and Preparation of the original draft of this manuscript. Z.Y.-N., G.A.K.; Conceptualisation, Methodology, Validation, and Project administration. Z.Y.-N., Y.A.; Software. Z.Y.-N., Z.M.; Resources. Z.Y.-N., G.A.K., Y.A., S.K., R.F.; Wrote, reviewed and edited the manuscript. R.F.; Consultation. G.A.K.; Supervision and funding acquisition. All authors read and approved the final manuscript.

## References

- Schietinger A, Greenberg PD. Tolerance and exhaustion: defining mechanisms of T cell dysfunction. *Trends Immunol.* 2014; 35(2): 51-60.
- Miggelbrink AM, Jackson JD, Lorrey SJ, Srinivasan ES, Waibl-Polania J, Wilkinson DS, et al. CD4 T-cell exhaustion: does it exist and what are its roles in cancer? *Clin Cancer Res.* 2021; 27(21): 5742-5752.
- Wherry EJ, Kurachi M. Molecular and cellular insights into T cell exhaustion. *Nat Rev Immunol.* 2015; 15(8): 486-499.
- Bonorino C, Mognol G. Editorial: T cell exhaustion. *Front Immunol.* 2020; 11: 920.
- Guram K, Kim SS, Wu V, Sanders PD, Patel S, Schoenberger SP, et al. A threshold model for T-Cell activation in the era of checkpoint blockade immunotherapy. *Front Immunol.* 2019; 10: 491.
- Torphy RJ, Schulick RD, Zhu Y. Newly emerging immune checkpoints: promises for future cancer therapy. *Int J Mol Sci.* 2017; 18(12): 2642.
- Yan T, Yu L, Shanguan D, Li W, Liu N, Chen Y, et al. Advances in pharmacokinetics and pharmacodynamics of PD-1/PD-L1 inhibitors. *Int Immunopharmacol.* 2023; 115: 109638.
- Simon B, Harrer DC, Schuler-Thurner B, Schaft N, Schuler G, Dörrie J, et al. The siRNA-mediated downregulation of PD-1 alone or simultaneously with CTLA-4 shows enhanced in vitro CAR-T-cell functionality for further clinical development towards the potential use in immunotherapy of melanoma. *Exp Dermatol.* 2018; 27(7): 769-778.
- Beane JD, Lee G, Zheng Z, Mendel M, Abate-Daga D, Bharathan M, et al. Clinical scale zinc finger nuclease-mediated gene editing of PD-1 in tumor infiltrating lymphocytes for the treatment of metastatic melanoma. *Mol Ther.* 2015; 23(8): 1380-1390.
- Su S, Zou Z, Chen F, Ding N, Du J, Shao J, et al. CRISPR-Cas9-mediated disruption of PD-1 on human T cells for adoptive cellular therapies of EBV positive gastric cancer. *Oncoimmunology.* 2016; 6(1): e1249558.
- Rupp LJ, Schumann K, Roybal KT, Gate RE, Ye CJ, Lim WA, et al. CRISPR/Cas9-mediated PD-1 disruption enhances anti-tumor efficacy of human chimeric antigen receptor T cells. *Sci Rep.* 2017; 7(1): 737.
- Nakazawa T, Natsume A, Nishimura F, Morimoto T, Matsuda R, Nakamura M, et al. Effect of CRISPR/Cas9-mediated PD-1-disrupted primary human third-generation CAR-T cells targeting EGFRvIII on in vitro human glioblastoma cell growth. *Cells.* 2020; 9(4): 998.
- Ureña-Bailén G, Lamsfus-Calle A, Daniel-Moreno A, Raju J, Schlegel P, Seitz C, et al. CRISPR/Cas9 technology: towards a new generation of improved CAR-T cells for anticancer therapies. *Brief Funct Genomics.* 2020; 19(3): 191-200.
- Nielsen C, Ohm-Laursen L, Barington T, Husby S, Lillevang ST. Alternative splice variants of the human PD-1 gene. *Cell Immunol.* 2005; 235(2): 109-116.
- Zhu X, Lang J. Soluble PD-1 and PD-L1: predictive and prognostic significance in cancer. *Oncotarget.* 2017; 8(57): 97671-97682.
- Khan M, Zhao Z, Arooj S, Fu Y, Liao G. Soluble PD-1: predictive, prognostic, and therapeutic value for cancer immunotherapy. *Front Immunol.* 2020; 11: 587460.
- Song MY, Park SH, Nam HJ, Choi DH, Sung YC. Enhancement of vaccine-induced primary and memory CD8(+) T-cell responses by soluble PD-1. *J Immunother.* 2011; 34(3): 297-306.
- Bartee MY, Dunlap KM, Bartee E. Tumor-localized secretion of soluble PD1 enhances oncolytic virotherapy. *Cancer Res.* 2017; 77(11): 2952-2963.
- Chamberlain CA, Bennett EP, Kverneland AH, Svane IM, Donia



- M, Met Ö. Highly efficient PD-1-targeted CRISPR-Cas9 for tumor-infiltrating lymphocyte-based adoptive T cell therapy. *Mol Ther Oncolytics*. 2022; 24: 417-428.
20. Stadtmayer EA, Fraietta JA, Davis MM, Cohen AD, Weber KL, Lancaster E, et al. CRISPR-engineered T cells in patients with refractory cancer. *Science*. 2020; 367(6481): eaba7365.
  21. Gapinske M, Luu A, Winter J, Woods WS, Kostan KA, Shiva N, et al. CRISPR-SKIP: programmable gene splicing with single base editors. *Genome Biol*. 2018; 19(1): 107.
  22. Mou H, Smith JL, Peng L, Yin H, Moore J, Zhang XO, et al. CRISPR/Cas9-mediated genome editing induces exon skipping by alternative splicing or exon deletion. *Genome Biol*. 2017; 18(1): 108.
  23. Togashi Y, Mizuuchi H, Tomida S, Terashima M, Hayashi H, Nishio K, et al. MET gene exon 14 deletion created using the CRISPR/Cas9 system enhances cellular growth and sensitivity to a MET inhibitor. *Lung Cancer*. 2015; 90(3): 590-597.
  24. Labun K, Montague TG, Krause M, Torres Cleuren YN, Tjeldnes H, Valen E. CHOPCHOP v3: expanding the CRISPR web toolbox beyond genome editing. *Nucleic Acids Res*. 2019; 47(W1): W171-W174.
  25. Concordet JP, Haeussler M. CRISPOR: intuitive guide selection for CRISPR/Cas9 genome editing experiments and screens. *Nucleic Acids Res*. 2018; 46(W1): W242-W245.
  26. Rajabzadeh A, Hamidieh AA, Rahbarizadeh F. Spinoculation and retronectin highly enhance the gene transduction efficiency of Mucin-1-specific chimeric antigen receptor (CAR) in human primary T cells. *BMC Mol Cell Biol*. 2021; 22(1): 57.
  27. Brinkman EK, Chen T, Amendola M, van Steensel B. Easy quantitative assessment of genome editing by sequence trace decomposition. *Nucleic Acids Res*. 2014; 42(22): e168.
  28. Nagasaki J, Togashi Y. A variety of 'exhausted' T cells in the tumor microenvironment. *Int Immunol*. 2022; 34(11): 563-570.
  29. Yu Y, Cui J. Present and future of cancer immunotherapy: a tumor microenvironmental perspective. *Oncol Lett*. 2018; 16(4): 4105-4113.
  30. Balança CC, Salvioni A, Scarlata CM, Michelas M, Martinez-Gomez C, Gomez-Roca C, et al. PD-1 blockade restores helper activity of tumor-infiltrating, exhausted PD-1hiCD39+ CD4 T cells. *JCI Insight*. 2021; 6(2): e142513.
  31. Bloemberg D, Nguyen T, MacLean S, Zafer A, Gadoury C, Gurnani K, et al. A high-throughput method for characterizing novel chimeric antigen receptors in Jurkat cells. *Mol Ther Methods Clin Dev*. 2020; 16: 238-254.
  32. Yang W, Chen PW, Li H, Alizadeh H, Niederkorn JY. PD-L1: PD-1 interaction contributes to the functional suppression of T-cell responses to human uveal melanoma cells in vitro. *Invest Ophthalmol Vis Sci*. 2008; 49(6): 2518-2525.
  33. Niu M, Liu Y, Yi M, Jiao D, Wu K. Biological characteristics and clinical significance of soluble PD-1/PD-L1 and exosomal PD-L1 in cancer. *Front Immunol*. 2022; 13: 827921.
  34. He L, Zhang G, He Y, Zhu H, Zhang H, Feng Z. Blockade of B7-H1 with sPD-1 improves immunity against murine hepatocarcinoma. *Anticancer Res*. 2005; 25(5): 3309-3313.
  35. Qiu H, Liu S, Xie C, Long J, Feng Z. Regulating immunity and inhibiting tumor growth by the recombinant peptide sPD-1-CH50. *Anticancer Res*. 2009; 29(12): 5089-5094.
  36. Zhang A, Sun Y, Wang S, Du J, Gao X, Yuan Y, et al. Secretion of human soluble programmed cell death protein 1 by chimeric antigen receptor-modified T cells enhances anti-tumor efficacy. *Cytotherapy*. 2020; 22(12): 734-743.
  37. Keir ME, Butte MJ, Freeman GJ, Sharpe AH. PD-1 and its ligands in tolerance and immunity. *Annu Rev Immunol*. 2008; 26: 677-704.
-